Formation of Two-Dimensional Sand Ripples under Laminar Shear Flow

Vincent Langlois and Alexandre Valance

GMCM, Université Rennes 1, Bâtiment 11A, 35042 Rennes, France
(Received 16 July 2004; published 20 June 2005)

The process of ripple formation on a two-dimensional sand bed sheared by a viscous fluid is investigated theoretically. The sand transport is described taking into account both the local bed shear stress (which is deduced from the resolution of the flow over a 2D deformed bed) and the local bed slope, via a simple nonlinear law. Within this model, a 2D linear stability analysis reveals that the most unstable mode is a longitudinal mode (i.e., it corresponds to sand ripples with a crest perpendicular to the flow). Most importantly, oblique modes are found to be unstable also and can couple to the most unstable mode in the nonlinear regime. We show through a weakly nonlinear analysis that this coupling gives birth to complex 2D steady sand patterns drifting along the flow at constant speed.

When a planar sand bed is sheared by a fluid, it becomes unstable and gives rise to bedform patterns. The description of sand patterns formed by the flow of wind or water still poses a great challenge to the community. Up to now, most theoretical works dealt with the linear stability analysis of a unidimensional sand bed [1–5], but very few investigated the formation of 2D sand patterns. We can cite the theoretical work of Vittori and Blondeaux [6] and the experimental studies and modeling of the Danish group [7,8]. These works pertain to the case of oscillating flows, but no one has investigated the stability of the 2D sand bed under a continuous shear flow. In nature, however, complex 2D sand patterns can be observed under a steady and continuous flow as, for example, on sandy river beds [9]. In this Letter, we present a theoretical study on the formation of 2D sand bed patterns under a laminar and steady shear flow. Several issues are addressed here: (i) Is the 2D linearly most unstable mode longitudinal (i.e., corresponding to ripples with a crest perpendicular to the flow direction)? (ii) What is the subsequent evolution of the sand bed? Does it remain invariant in the direction perpendicular to the flow or does it exhibit transverse instabilities giving rise to complex 2D patterns?

Our analysis is based on a classical description of sand transport. The rate of sand transport is evaluated as a function of both the local bed shear stress (which is derived from the resolution of the flow over a deformed sand surface) and the local bed slope, using a standard semi-empirical law [10]. The evolution of the sand bed is then deduced via the mass conservation of sand grains. We first investigated the linear stability of such a 2D sand bed and derived an explicit expression for the growth rate of the unstable modes as a function of the physical parameters of the system (i.e., the shear rate γ, the fluid viscosity ν, the grain diameter d, etc.). We found that the most unstable mode is longitudinal and therefore corresponds to sand ripples with a crest perpendicular to the flow direction. Most importantly, oblique modes are found to be unstable also and can couple in a resonant way to the most unstable mode in the nonlinear regime. In particular, we show that

the nonlinear coupling of a resonant triad composed of one longitudinal mode and two symmetric oblique modes gives birth to a rich variety of 2D steady bedforms, such as brick or hexagonal patterns [11]. This last result contrasts with what is observed experimentally for a quasi-1D sand bed [12,13] where the ripple pattern does not reach a steady state but exhibits a coarsening process.

We consider a Newtonian and viscous fluid flowing over a sand surface described by its height $h(x, y, t)$. The flow is unidirectional along the x direction and has a thickness L. We choose a Couette flow configuration; that is, the vertical velocity profile is linear (in the case of a flat sand bed) and the shear rate γ is imposed. The equations of motion for the fluid read

$$\begin{cases} \rho \frac{\partial \mathbf{u}}{\partial t} + \rho(\mathbf{u} \cdot \boldsymbol{\nabla})\mathbf{u} = -\boldsymbol{\nabla}p + \eta\nabla^2\mathbf{u}, \\ \boldsymbol{\nabla} \cdot \mathbf{u} = 0, \end{cases} \quad (1)$$

$\mathbf{u} = (u, v, w)$ being the fluid velocity, p the pressure, ρ the volumetric mass of the fluid, and η its dynamic viscosity ($\nu = \eta/\rho$ being the kinematic viscosity). These equations are supplemented with the following boundary conditions: $\mathbf{u} = \mathbf{0}$ at the bed surface and $\mathbf{u} = (\gamma L, 0, 0)$ at the height $z = L$.

The transport of sediment is induced by the bed shear stress σ (i.e., the flow shear stress calculated at the sand surface), but its precise evaluation is not a simple matter since it involves intricate and complex processes such as grain-grain and fluid-grain interactions. Up to now, there is no sound theoretical description for the transport of particles. Therefore, we use a generic law inspired from those established empirically for a one-dimensional sand bed [10].

Let us first introduce a dimensionless bed shear stress vector defined by $\boldsymbol{\Theta} = \frac{\boldsymbol{\sigma}}{\rho g(s-1)d}$, where $s = \rho_g/\rho$ is the relative density of the sediment compared to that of the fluid, $\boldsymbol{\sigma}$ the bed shear stress, g the gravitational acceleration, and d the diameter of the grains. The modulus of this dimensionless vector is referred to as the Shields number. The horizontal mass transport rate [$\mathbf{q} = (q_x, q_y)$] is as-

sumed to obey the following law:

$$\mathbf{q} = q_b\left[\left\|\boldsymbol{\Theta}_\mathbf{h} - \frac{\Theta_{c_0}}{\mu_s}\boldsymbol{\nabla}h\right\| - \Theta_{c_0}\right]^m \frac{\boldsymbol{\Theta}_\mathbf{h} - \frac{\Theta_{c_0}}{\mu_s}\boldsymbol{\nabla}h}{\|\boldsymbol{\Theta}_\mathbf{h} - \frac{\Theta_{c_0}}{\mu_s}\boldsymbol{\nabla}h\|}, \quad (2)$$

where $q_b = c\sqrt{(s-1)gd^3}$ (c is a numerical constant), $\boldsymbol{\Theta}_h$ is the horizontal projection of the dimensionless bed shear stress, Θ_{c_0} is the critical value of the Shields number to set grains into motion on a flat horizontal sand bed, and μ_s is the internal friction coefficient of the material. The exponent m is chosen to be equal to 3/2 as in the Meyer-Peter law [10]. Note also that the term raised to the power m must be positive or zero. If this term is negative, the sand transport is not possible and is therefore reduced to zero. Equation (2) is a 2D version of the standard transport laws established for a one-dimensional sand bed. It is composed of two terms, one evaluating the rate of sand transport and the other giving its direction in the horizontal plane. The rate of sand transport results from the competition between the different forces acting on the grains from the bed surface [10]: the drag force (proportional to the bed shear stress), the gravitational force, and the friction force between the moving grains and the static bed (estimated by the Coulomb law). For a flat bed (i.e., $\nabla h = 0$), the sand transport rate is simply a function of the Shields number reduced by the critical Shields number ($\|\boldsymbol{\Theta}_\mathbf{h}\| - \Theta_{c0}$). When the bed is tilted downstream (upstream), the sand transport rate is clearly increased (decreased). This bed slope effect is taken into account by the presence of the term proportional to ∇h. The second term, which indicates the local direction of grain motion, is simply given by the sum of the driving forces (drag force plus gravity).

Finally, the model is closed by the mass conservation equation for the grains:

$$\frac{\partial h}{\partial t} = -\boldsymbol{\nabla} \cdot \mathbf{q}. \quad (3)$$

The trivial stationary solution of these model equations corresponds to a simple linear shear flow over a flat horizontal sand bed. The velocity profile is therefore given by $u_0(z) = \gamma z$ and the transport rate by $|\mathbf{q}_0| = c\sqrt{(s-1)gd^3} \times (\Theta_0 - \Theta_{c_0})^m$, where $\Theta_0 = \nu\gamma/[g(s-1)d]$ is the Shields number in the case of a flat bed.

In the next development, we use the classical hypothesis of quasistationarity; that is, the typical hydrodynamical time is much smaller than the typical morphological time. The hydrodynamic equations are therefore solved over a fixed sand bed surface.

In order to study the linear stability of the planar sand bed, we assume that the sand surface presents a perturbation of small amplitude, $h(x, y, t) = h_1 e^{i(k_x x + k_y y) + \omega t}$, where $\mathbf{k} = k_x\mathbf{e_x} + k_y\mathbf{e_y}$ is the wave vector of the perturbation, and ω its growth rate. We first have to calculate the flow perturbation, the bed surface being kept fixed. The perturbed flow quantities can be written as

$$(u, v, w, p) = (u_0, 0, 0, p_0)$$
$$+ (U_1, V_1, W_1, P_1)e^{i(k_x x + k_y y) + \omega t}. \quad (4)$$

Keeping only the linear terms in the hydrodynamic equations, we get the following coupled equations for U_1, V_1, W_1, and P_1:

$$ik_x\gamma z U_1 + \gamma W_1 + ik_x\frac{P_1}{\rho} = \nu(\partial_z^2 - k_x^2 - k_y^2)U_1, \quad (5)$$

$$ik_x\gamma z V_1 + ik_y\frac{P_1}{\rho} = \nu(\partial_z^2 - k_x^2 - k_y^2)V_1, \quad (6)$$

$$ik_x\gamma z W_1 + \frac{1}{\rho}\partial_z P_1 = \nu(\partial_z^2 - k_x^2 - k_y^2)W_1, \quad (7)$$

$$ik_x U_1 + ik_y V_1 + \partial_z W_1 = 0, \quad (8)$$

with the following boundary conditions:

$$z = 0: U_1 = -\gamma h_1, \quad V_1 = 0, \quad W_1 = 0;$$
$$z = L: U_1 = 0, \quad V_1 = 0, \quad W_1 = 0. \quad (9)$$

Combining Eqs. (5)–(8) gives a closed equation for W_1:

$$[\nu(\partial_z^2 - k^2) - ik_x\gamma z](\partial_z^2 W_1 - k^2 W_1) = 0, \quad (10)$$

whose solution can be expressed in terms of the Airy functions Ai and Bi as

$$W_1(z) = a_1 e^{kz} + b_1 e^{-kz} + \frac{e^{kz}}{2k}$$
$$\times \int_0^z d\zeta e^{-k\zeta}[a_2\text{Ai}(\zeta') + b_2\text{Bi}(\zeta')] - \frac{e^{-kz}}{2k}$$
$$\times \int_0^z d\zeta e^{k\zeta}[a_2\text{Ai}(\zeta') + b_2\text{Bi}(\zeta')], \quad (11)$$

where a_i and b_i are integration constants, $k = \sqrt{k_x^2 + k_y^2}$, and $\zeta' = e^{i\pi/6}(k_x l_\nu)^{-2/3}(k_x\zeta - ik^2 l_\nu^2)$. We recall that $l_\nu = \sqrt{\nu/\gamma}$ is the viscous length. In the same way, U_1 and V_1 can also be calculated analytically and expressed in terms of the Airy functions and W_1. For the sake of brevity, we do not give their explicit expressions here.

We are now in position to calculate the perturbed bed shear stress $\boldsymbol{\sigma}_1$ ($\boldsymbol{\sigma} = \boldsymbol{\sigma}_0 + \boldsymbol{\sigma}_1 e^{i(k_x x + k_y y) + \omega t}$). In order to simplify further calculations, we focus on the situation where the width L of the flow is much greater than the dimensions of the bed perturbation. In this case, one can obtain approximate analytical expressions for $\boldsymbol{\sigma}_1$. In particular, in the long wavelength limit (i.e., $kl_\nu \ll 1$), we get

$$\frac{\sigma_{1x}}{\sigma_0 h_1} = e^{i\pi/6}l_\nu^{-2/3}k_x^{1/3}\frac{1.07k_x^2 - 0.73k_y^2}{k_x^2 + k_y^2} + O(kl_\nu), \quad (12)$$

$$\frac{\sigma_{1y}}{\sigma_0 h_1} = 0.34e^{i\pi/6}l_\nu^{-2/3}\frac{k_x^{4/3}k_y}{k_x^2 + k_y^2} + O(kl_\nu), \quad (13)$$

where $\sigma_0 = \eta\gamma$.

The growth rate of the bed perturbation can easily be derived by linearizing the transport law [Eq. (2)] and using mass conservation Eq. (3). We get

$$\omega = -ik_x m\mu^{m-1}\Theta_{c_0}^m\left((1+\mu)\frac{\sigma_{1x}}{\sigma_{10}} - \frac{ik_x}{\mu_s}\right)$$

$$- ik_y\mu^m\Theta_{c_0}^m\left(\frac{\sigma_{1y}}{\sigma_{10}} - \Theta_{c_0}(1+\mu)\frac{ik_y}{\mu_s}\right), \quad (14)$$

where we introduced the parameter $\mu = (\Theta_0 - \Theta_{c_0})/\Theta_{c_0}$ which is referred to as the relative shear stress excess. Equation (14) consists of two terms: the first one (the second one) involves the bed shear stress in the x direction (in the y direction). Referring to expressions (12) and (13), we note that σ_{1x} plays a destabilizing role, whereas σ_{1y} stabilizes the sand bed for small k. As can be seen in Fig. 1 where we plotted the marginal stability curve for different values of μ, pure longitudinal modes are unstable at small k while pure transverse modes are stable. At larger k, the longitudinal modes are stabilized by the gravitational effect (terms proportional to k_x/μ_s), as found in the 1D stability analysis fully detailed in [5,14]. Indeed, the gravitational effect enhances (lowers) the critical Shields number for the onset of grain motion on upward slopes (on downward slopes); this prevails for large slopes (i.e., for large k) and tends to smooth the sand bed surface. The most dangerous mode is found to be longitudinal (i.e., $k_y = 0$) and therefore corresponds to sand ripples invariant in the direction perpendicular to the flow. This is the same result as found by Roos and Blondeaux [11] with an oscillatory flow. This finding seems rather consistent with the experimental observations made for unidirectional flows in a wide channel: the structures appearing at the first stages of the instability have crests perpendicular to the flow, before bifurcating to more complex patterns [15]. The wavelength of the most dangerous mode can easily be calculated, and one finds $\lambda_{\max} = 30l_\nu/\mu_s^{3/2}(1+\mu)^{3/2}$.

Perhaps, the most interesting result is the existence of unstable oblique modes. Although these modes are not expected to prevail in the linear regime (since their growth rate is smaller than that of the most dangerous mode), we may wonder whether they play an important role in the nonlinear regime. Could they, for example, couple to a longitudinal mode in a resonant way and enter the dynamics of the sand surface? In that case what kind of 2D sand patterns can be expected?

To solve these issues, we performed a weakly nonlinear analysis. We focused on the nonlinear interaction of three
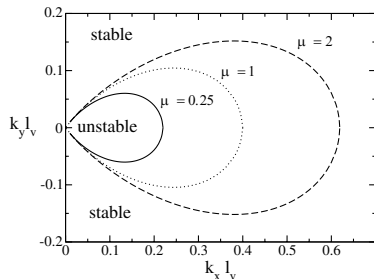
FIG. 1.   Marginal stability curves for different values of μ.

components of the sand bed perturbation, each characterized by a wave vector $\mathbf{k}_i$ ($i = 1, 2, 3$) and hence proportional to $e^{i\mathbf{k}_i \cdot \mathbf{r}}$. The interaction of these perturbation components is particularly strong when adding two of the wave vectors gives the third one: $\mathbf{k}_1 = \mathbf{k}_2 + \mathbf{k}_3$. We study here the superposition of one longitudinal mode and two symmetrical oblique modes, of respective wave vectors $\mathbf{k}_1 = k_x\mathbf{e}_x$, $\mathbf{k}_2 = \frac{1}{2}k_x\mathbf{e}_x + k_y\mathbf{e}_y$, $\mathbf{k}_3 = \frac{1}{2}k_x\mathbf{e}_x - k_y\mathbf{e}_y$. Let us therefore consider the following structure for the sand bed surface perturbation:

$$h(x, y) = \varepsilon(A_1e^{i\mathbf{k}_1\cdot\mathbf{r}} + A_2e^{i\mathbf{k}_2\cdot\mathbf{r}} + A_3e^{i\mathbf{k}_3\cdot\mathbf{r}} + \text{c.c.})$$
$$+ \varepsilon^2(B_1e^{i\mathbf{k}_1\cdot\mathbf{r}} + B_2e^{i\mathbf{k}_2\cdot\mathbf{r}} + B_3e^{i\mathbf{k}_3\cdot\mathbf{r}} + \text{c.c.}$$
$$+ \text{terms proportional to } e^{2\mathbf{k}_1\cdot\mathbf{r}}, e^{2\mathbf{k}_2\cdot\mathbf{r}}, \ldots)$$
$$+ O(\varepsilon^3), \quad (15)$$

where ε is a small parameter defined as $\omega(\mathbf{k}_i) = \alpha_i\varepsilon$ (where α_i are coefficients close to unity). The further analysis is, indeed, performed in the vicinity of the marginal stability region [i.e., the wave vectors k_i are chosen sufficiently close to the marginal stability curve where $\omega(\mathbf{k}) = 0$]. The principle of the nonlinear analysis is to expand all variables of the problem in power of the small parameter ε and to solve successively at each order. The interesting result comes to order ε^2 where we get three nonlinear coupled equations for the complex amplitudes A_1, A_2, and A_3 [6]:

$$\dot{A}_1 = \omega_1A_1 + K_1A_2A_3, \quad (16)$$

$$\dot{A}_2 = \omega_2A_2 + K_2A_1A_3^*, \quad (17)$$

$$\dot{A}_3 = \omega_3A_3 + K_3A_1A_2^*. \quad (18)$$

The coupling coefficients K_1, K_2, and K_3 can be calculated analytically. We find

$$K_1 = -\frac{3i}{4}k_x\Theta_{c0}^{3/2}\mu^{-1/2}\left[(1+\mu)^2\frac{\tau_2\tau_3}{\sigma_0^2}\right.$$
$$\left. - ik_x\frac{(1+\mu)}{\mu_s}\frac{\tau_2}{\sigma_0} - \frac{k_x^2}{4\mu_s^2}\right], \quad (19)$$

$$K_{2,3} = -\frac{3i}{8}k_x\Theta_{c0}^{3/2}\mu^{-1/2}\left[(1+\mu)^2\frac{\tau_1\tau_{3,2}^*}{\sigma_0^2} + \frac{k_x^2}{2\mu_s^2}\right.$$
$$\left. - i(1+\mu)\frac{k_x}{\mu_s}\left(\frac{\tau_{3,2}^*}{\sigma_0} - \frac{\tau_1}{2\sigma_0}\right)\right]. \quad (20)$$

We introduced the notations $\omega_i = \omega(\mathbf{k}_i)$ and $\tau_i = \sigma_{1x}(\mathbf{k}_i)$. Because of symmetry, $\tau_2 = \tau_3$ and $\omega_2 = \omega_3$ so that equations for A_2 and A_3 are identical. Introducing the real amplitude and the phase of the perturbations, $A_i = a_ie^{i\phi_i}$, we can deduce real equations. There is a plethora of possibilities, but we limit ourselves to a typical situation where $a_2 = a_3$ and $\phi_2 = \phi_3$. In this case, the system reduces to coupled equations for a_1, a_2, and the phase shift $\Delta\phi = 2\phi_2 - \phi_1$:

$$\dot{a}_1 = \text{Re}(\omega_1)a_1 + \kappa_1a_2^2, \quad (21)$$
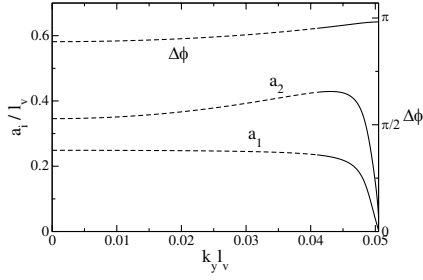
FIG. 2.   Amplitudes a_1 and a_2 and phase shift $\Delta\phi$ correspond-ing to steady state solutions as a function k_y for a fixed value of k_x. The continuous parts of the curves indicate the region where the solutions are stable with respect to fluctuations of amplitudes and phases. Parameters: $k_x l_v = 0.1$ and $\mu = 0.1$.

$$\dot{a}_2 = \mathrm{Re}(\omega_2)a_2 + \kappa_2 a_1 a_2, \tag{22}$$

$$\Delta\dot{\phi} = \mathrm{Im}(2\omega_2 - \omega_1) - \left[2\,\mathrm{Re}(K_2)a_1 - \mathrm{Re}(K_1)\frac{a_2^2}{a_1}\right]$$
$$\times \sin(\Delta\phi) + \left[2\,\mathrm{Im}(K_2)a_1 - \mathrm{Im}(K_1)\frac{a_2^2}{a_1}\right]\cos(\Delta\phi) \tag{23}$$

with $\kappa_i = \mathrm{Re}(K_i)\cos(\Delta\phi) + (-1)^i \mathrm{Im}(K_i)\sin(\Delta\phi)$ ($i = 1, 2$). When the amplitudes a_i are sufficiently small, the linear terms dominate and the modes grow or decay ex-ponentially depending on the sign of the growth rate. The nonlinear terms enhance or saturate the exponential growth according to the sign of the coupling coefficients κ_1 and κ_2, which depends in a complicated way on the chosen modes and on their relative phase $\Delta\phi$. If κ_1 or κ_2 is positive, a_1 or a_2 will have an explosive growth (i.e., faster than an exponential one) and our nonlinear analysis will break down. On the other hand, if κ_1 and κ_2 are both negative, we can expect a 2D steady pattern to form. These steady patterns correspond to the stationary solu-tions of Eqs. (21)–(23) (i.e., $\dot{a}_1 = \dot{a}_2 = \Delta\dot{\phi} = 0$). We have determined the domain of existence of these solutions in the parameter space (μ, **k**) and have found that in the unstable region [i.e., where $\omega(\mathbf{k})$ is positive], there always exist such stationary solutions. We present in Fig. 2 typical evolutions of a_1, a_2, and $\Delta\phi$ as a function of k_y for fixed

values of k_x and μ. It should be noted that the range of variation of k_y is restricted to the unstable domain. Figure 3 gives examples of ripple patterns obtained for different values of the ratio k_x/k_y and the phase shift $\Delta\phi$. These patterns drift along the flow direction at a constant speed v_d given by $v_d = \dot{\phi}_1/k_x$.

In summary, we have shown, using a model based on the resolution of the flow over a 2D deformed sand bed coupled to a law for sand transport, the existence of 2D stationary ripples patterns. They result from the nonlinear coupling of a resonant triad of perturbation modes. We considered here the simple situation of a triad composed of one longitudinal mode and two symmetrical oblique modes, and found that the sand bed surface can exhibit a large variety of 2D structures depending on the wave num-bers and phase shift of the different modes. However, an important issue remain to be addressed: What is the final 2D pattern selected by the system for a given shear rate? To answer this question, a full numerical nonlinear analysis is needed. Parallel to this, it would also be highly desirable to conduct experiments on sand ripples in large channels. At last, we may wonder how our results could be applied to natural flows that are generally turbulent. In turbulent flow configurations, our analysis, of course, breaks down; how-ever, one may expect the mechanisms leading to 2D sand patterns to be similar in laminar and turbulent flows be-cause the origin of sand bed instability has nothing to do with the turbulent feature of a flow.

FIG. 3.   Examples of bedforms: left $\Delta\phi = \pi/2$, $k_x/k_y = 4$, $a_1 = a_2$ (brick pattern); right $\Delta\phi = 2\pi/3$, $k_x/k_y = 2$, $a_1 = a_2/2$ (hexagonal pattern).

[1] J. F. Kennedy, J. Fluid Mech. **16**, 521 (1963).
[2] K. J. Richards, J. Fluid Mech. **99**, 597 (1980).
[3] B. M. Sumer and M. Bakioglu, J. Fluid Mech. **144**, 117 (1984).
[4] S. E. Coleman and J. D. Fenton, J. Fluid Mech. **418**, 101 (2000).
[5] F. Charru and H. Mouilleron-Arnould, J. Fluid Mech. **452**, 303 (2002).
[6] G. Vittori and P. Blondeaux, J. Fluid Mech. **239**, 23 (1992).
[7] J. L. Hansen, M. V. Hecke, C. Ellegaard, K. H. Andersen, T. Bohr, and T. Sam, Phys. Rev. Lett. **87**, 204301 (2001).
[8] K. H. Andersen, M. Abel, J. Krug, C. Ellegaard, L. R. Soendergaard, and J. Udesen, Phys. Rev. Lett. **88**, 234302 (2002).
[9] A. W. Wilbers and W. B. Ten Brinke, Sedimentology **50**, 1013 (2003).
[10] J. Fredsøe and R. Deigaard, *Mechanics of Coastal Sediment Transport* (World Scientific, Singapore, 1992).
[11] P. C. Roos and P. Blondeaux, J. Fluid Mech. **447**, 227 (2001).
[12] A. Betat, C. A. Kruelle, V. Frette, and I. Rehberg, Eur. Phys. J. E **8**, 465 (2002).
[13] T. Loiseleux, D. Doppler, P. Gondret, and M. Rabaud (private communication).
[14] A. Valance and V. Langlois, Eur. Phys. J. B **43**, 283 (2005).
[15] V. Langlois and A. Valance (unpublished).